EUROPEAN ORGANIZATION FOR NUCLEAR RESEARCH

CERN-Nufact-Note-059

Muon Front-End without Cooling

K. Hanke

Abstract

In this note a muon front-end without cooling is presented. The muons are captured, rotated and accelerated to the energy needed for injection into the first muon recirculator. The cavity parameters are consistent with those used for the CERN reference scenario [1]. The number of muons obtained per year is roughly one order of magnitude less than the one obtained with the cooling channel. Therefore such a scheme could be a first step to a neutrino factory keeping the option of later upgrade.

Geneva, Switzerland
December 21, 2000

1 Introduction

In the design of a muon front-end for a future neutrino factory cooling is one of the most challenging issues. Theoretical and experimental studies are underway to examine the feasibility of ionization cooling in such an application. In this note we present a muon front-end without cooling. It is based on the same cavity parameters as the CERN cooling channel described elsewhere [1]. Therefore the two schemes are compatible and a scheme without cooling could be a first step towards a neutrino factory. The scheme proposed here is not to be confused with the one described in [2], for which it has been shown that it does not give any reasonable muon yield.

As it has been shown that cooling reduces the transverse emittance by a factor of 4 in each plane, taking out the cooling will reduce the muon yield by approximately a factor of 16. Careful modeling of the longitudinal optics can partially compensate for this and in the end lead to a reasonable number of muons per year.

In a first section the subject of the recirculator acceptance will be addressed. Then the various sections of the front-end will be described in detail: decay channel, capture and rotation in longitudinal phase space and subsequent acceleration of the muons up to 2 GeV kinetic energy. The simulations presented here have been performed with the code *PATH* [3]. Transverse and longitudinal constraints have been included to make the simulation as complete as possible. All simulations have been done under exactly the same conditions (target data, rf and solenoid modeling) as those done for the CERN cooling channel.

2 Recirculator Acceptance

The figure of merit for any front-end design is the muon yield within the acceptance of the first muon recirculator at injection. For the CERN reference scenario the transverse phase space acceptance is given by **1.5 π cm rad (normalized)** [4].

In the longitudinal plane the bunch area A in the decay ring has to be matched. As A is an invariant upon transfer from the first muon recirculator to the second and to the decay ring (longitudinal matching during the transfer is not possible), this is hence the parameter to be matched at injection into the first recirculator. Depending on what convention is used the value of A is given by

$$A = \pi \sigma_e \sigma_z E/c$$

where its value is **0.0185 eVs** [5], or by

$$A = \pi 2\sigma_e 2\sigma_z E/c$$

in which case its value is **0.074 eVs** [4, 6]. Here, σ_e is the relative rms energy spread and σ_z is the rms bunch length. The second definition is the one which is generally used. We will however give the muon yield for both values.

It is useful to assume a value for the recirculator acceptance in order to estimate the muon yield per year and to optimize the front-end optics. However, the real acceptance of the muon recirculators and hence the final muon yield can only be found by tracking the particle distribution at the exit of the front-end through these machines. This will be subject of future work.

3 Target Data

The target data have been generated with FLUKA for a 2.2 GeV proton beam instantaneously impinging on a 26 mm Hg target in a 20 T solenoid field [7]. As the real target is supposed to be 260 mm long, a linear extrapolation is done when calculating the muon yield in Section 6. It should be stressed that the target data file used for these simulations is the same that has been used for the simulation of the cooling channel [1].

4 Lay-out of the Front-End

The muon front-end consists of five main sections: decay channel, phase rotation, acceleration at f=44 MHz, acceleration at f=88 MHz and acceleration at f=176 MHz. Figure 1 shows schematically the lay-out of the front-end. In the following sections we summarize the main parameters of the various sections.

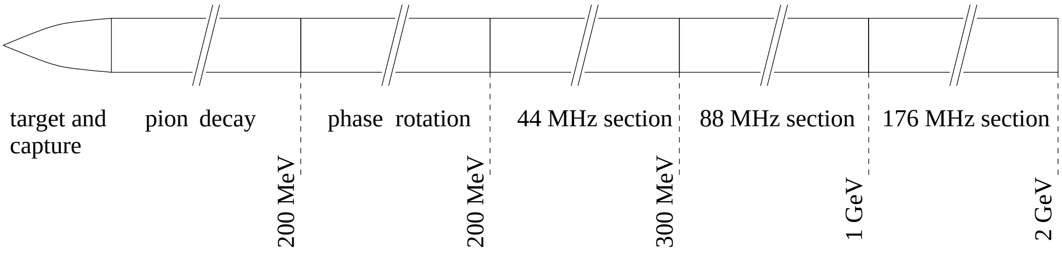

Figure 1: Schematic lay-out of the muon front-end without cooling.

4.1 Decay Channel

The decay channel allows practically all pions to decay into muons. The lay-out of the decay channel is exactly the same as for the CERN reference scenario [1]. Table 1 gives the main parameters of this section. The particle distribution in longitudinal phase space at the exit of the decay channel is shown in Fig. 2. As can be seen, the total muon distribution covers a

total length [m]	30
solenoid field [kG]	18
aperture [cm]	60

Table 1: Lay-out of the decay channel.

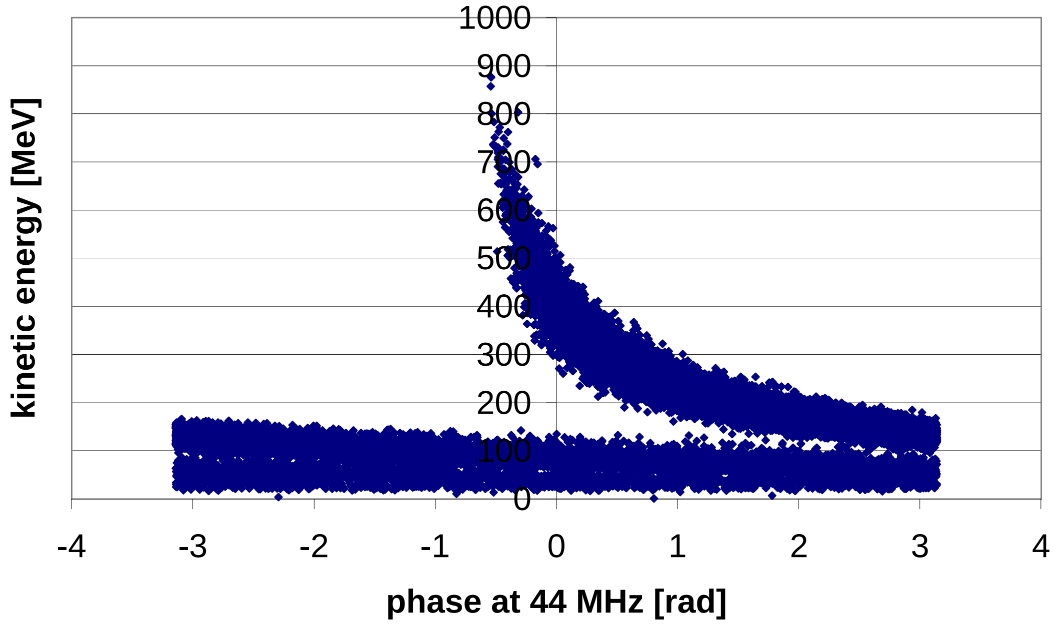

Figure 2: Longitudinal phase space distribution of muons at the exit of the decay channel.

large energy range and by no means one can inject the whole set of particles into any subsequent accelerator. Therefore, a cut in kinetic energy is performed and only particles between $E_{kin} = 100$ MeV and $E_{kin} = 300$ MeV are considered in the following simulations.

4.2 Phase Rotation

The phase rotation section reduces the energy spread of the selected subset of muons. This is performed by a series of cavities at f=44 MHz and appropriate setting of the phase. The lay-out of this section is identical with the one used for the CERN cooling channel (see Tab. 2). The particle distribution in longitudinal phase space at the exit of the phase rotation section is shown in Fig. 3.

total length [m]	38
solenoid field [kG]	18
aperture [cm]	60
frequency [MHz]	44
cavity length [m]	1.0
gradient [MV/m]	2.0
synchronous phase [deg]	variable
kinetic energy [MeV]	200

Table 2: Lay-out of the phase rotation section.

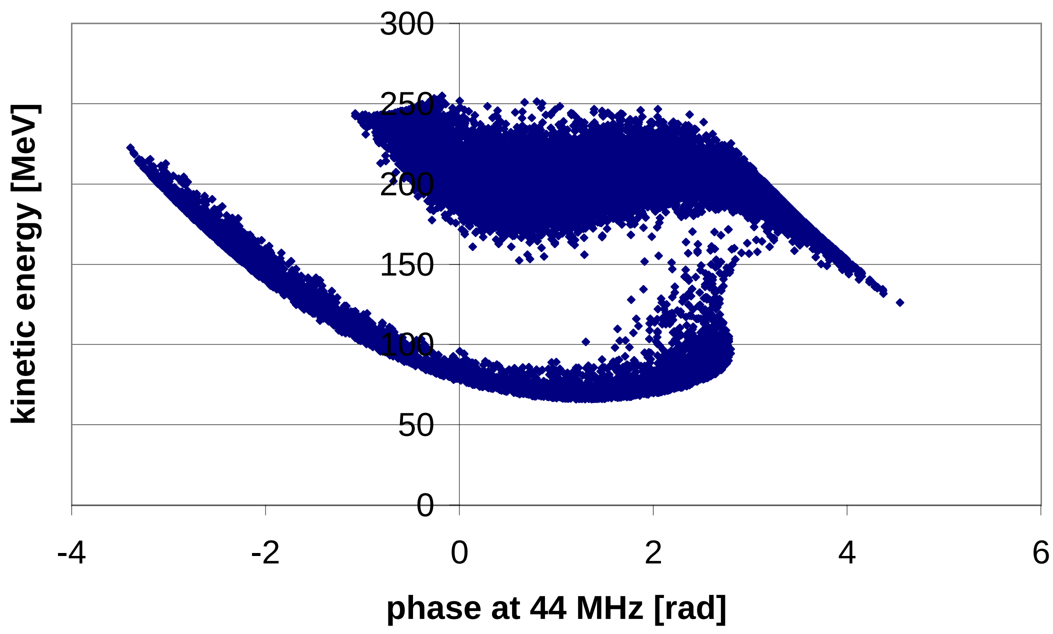

Figure 3: Longitudinal phase space distribution of muons at the exit of the phase rotation section.

4.3 Acceleration at 44 MHz

In a first acceleration section at f=44 MHz muons are accelerated on crest to about 300 MeV kinetic energy. The parameters of the section are given in Tab. 3. The particle distribution in longitudinal phase space at the exit of this section is shown in Fig. 4.

total length [m]	44
solenoid field [kG]	22.7
aperture [cm]	60
frequency [MHz]	44
cavity length [m]	1.0
gradient [MV/m]	2.0
synchronous phase [deg]	0
kinetic energy [MeV]	200 - 300

Table 3: Lay-out of the 44 MHz acceleration section.

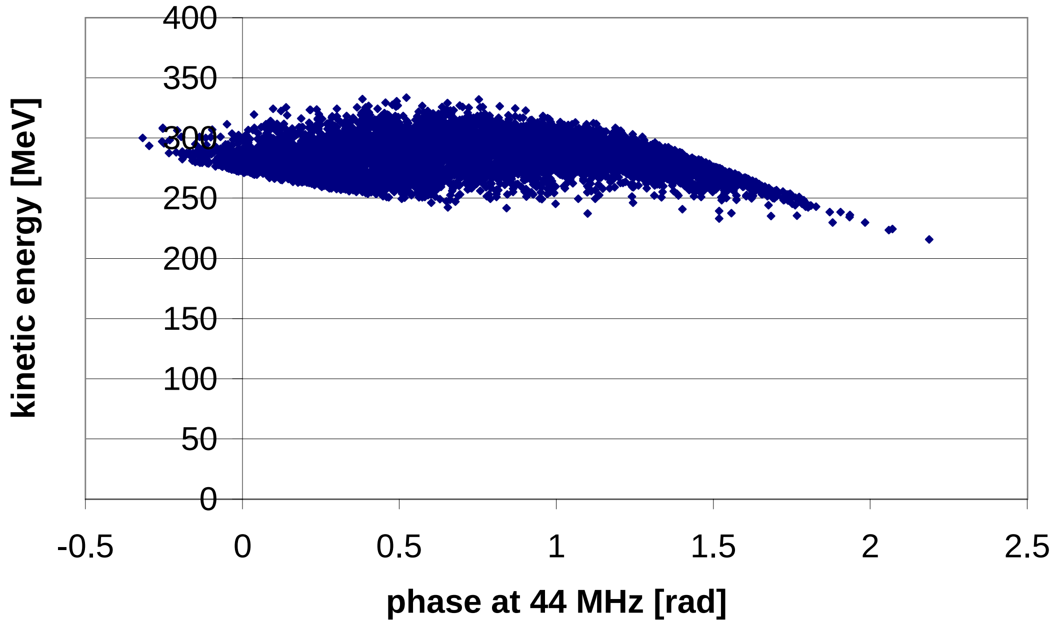

Figure 4: Longitudinal phase space distribution of muons at the exit of the 44 MHz section.

4.4 Acceleration at 88 MHz

The second acceleration section is at f=88 MHz and accelerates the beam to a kinetic energy of about 1 GeV.

The change of frequency from 44 MHz to 88 MHz implies a change of the aperture from 60 cm diameter to 30 cm diameter. In order to match the beam envelope to the smaller aperture, a matching section is included which consists of a 0.5 m long solenoid at 40 kG and a drift space of 0.22 m.

The phase of the cavities in this section alternates between $+45^o$ and -45^o to ensure that the particle distribution does not rotate in the longitudinal phase space but stays flat thus avoiding an excessive increase in energy spread. The parameters are given in Tab. 4. The particle distribution in longitudinal phase space for different steps of the acceleration is shown in Fig. 5.

total length [m]	280
solenoid field [kG]	50.0
aperture [cm]	30
frequency [MHz]	88
cavity length [m]	0.5
gradient [MV/m]	4.0
synchronous phase [deg]	± 45
kinetic energy [MeV]	300 - 1000

Table 4: Lay-out of the 88 MHz acceleration section.

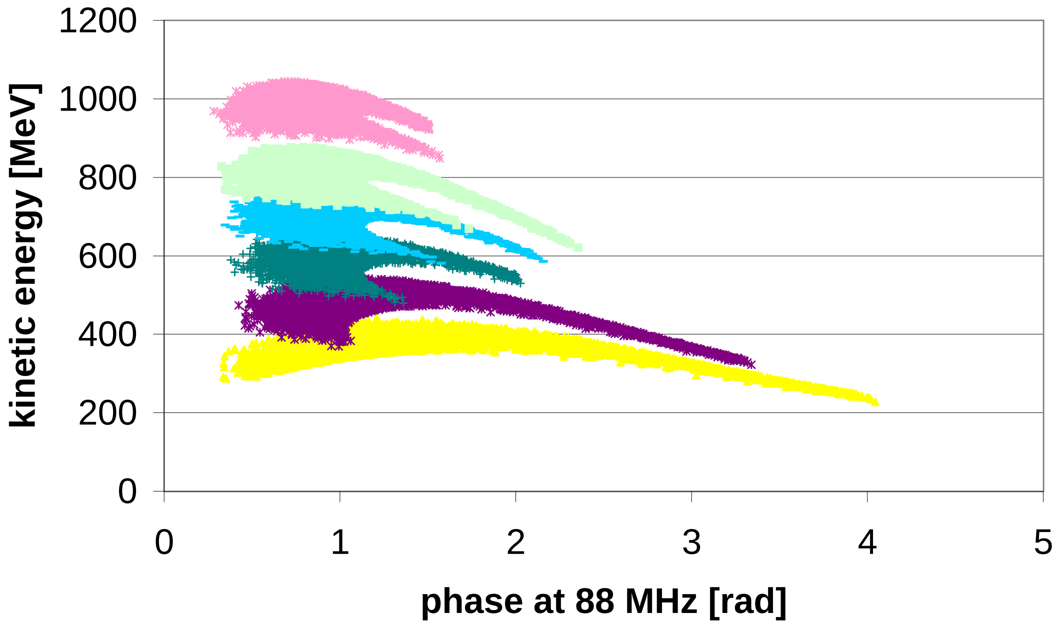

Figure 5: Longitudinal phase space distribution of muons during acceleration to 1 GeV. Note that phase cuts are performed for the sake of setting the synchronous phase correctly in the simulation.

There is presently no dedicated matching section between the section at f=88 MHz and the following one at f=176 MHz.

4.5 Acceleration at 176 MHz

The final acceleration section is at f=176 MHz and brings the beam to the injection energy of 2 GeV. The synchronous phase in this section is set to 0^o which yields optimum acceleration efficiency. The parameters of the final acceleration section are given in Tab. 5. The particle distribution in longitudinal phase space for different steps of the acceleration is shown in Fig. 6.

5 Transverse Optics

Appropriate solenoid settings ensure maximum transmission of the muons through the channel. The maximum achievable field is for the given geometry around 50 kG which still leaves some safety margin [8]. There are however losses, in particular at the transitions between sections with different apertures. The individual solenoid settings for the various sections are

total length [m]	112
solenoid field [kG]	60.0
aperture [cm]	20
frequency [MHz]	176
cavity length [m]	0.5
gradient [MV/m]	10.0
synchronous phase [deg]	0
kinetic energy [MeV]	1000 - 2000

Table 5: Lay-out of the 176 MHz acceleration section.

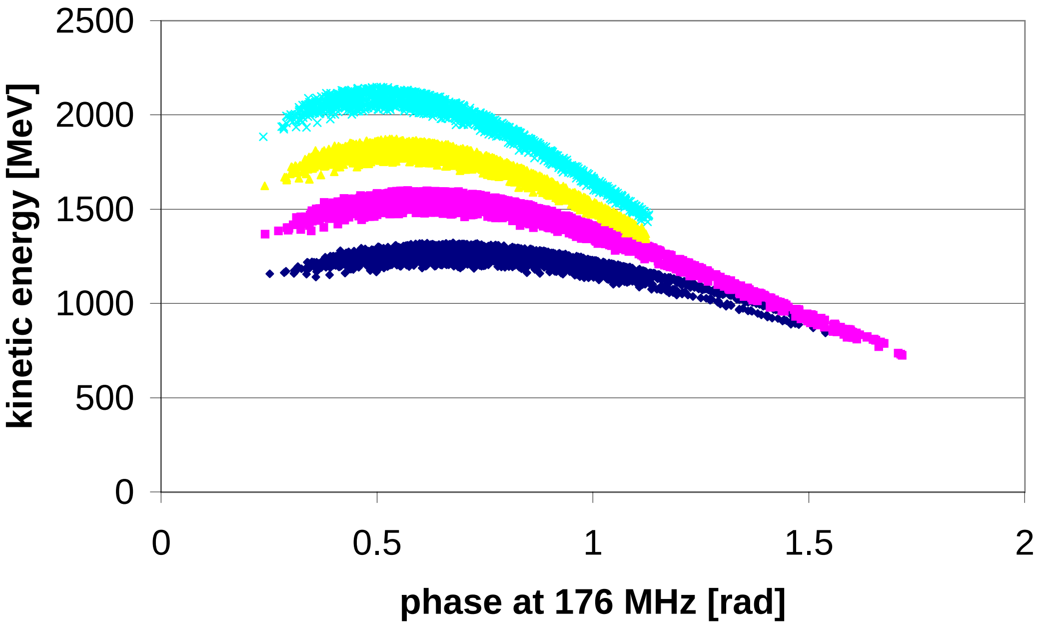

Figure 6: Longitudinal phase space distribution of muons during acceleration to 2 GeV. Again, phase cuts ensure correct setting of the synchronous phase.

found in the corresponding parameter tables.
At present, the *PATH* model uses a hard-edge approximation with fringe fields for the solenoid fields. The cavity model is a zero-length element with a field computed according to the bore radius. In order to represent better the real configuration , i. e. cavities with solenoids around the bores, at least a preliminary cavity and solenoid design is required. The field maps have then to be computed and included in the *PATH* model. This will be subject of further studies.
A formalism for matching in the transverse phase space between different sections of a solenoid channel is being developed and will be integrated in *PATH* [9].

6 Muon Yield

The muon yield within the acceptance limits given in Section 2 has been computed at the exit of the various stages of the simulation. The muons within the acceptance limits have been converted into muons/year, assuming a number of 10^{23} protons per year on the target. The results are given in Tab. 6. These values are to be compared to the corresponding values obtained for the CERN reference scenario, i.e. 2×10^{20} μ/year for an acceptance of 0.0185 eVs and 1.5 π cm rad and 5.5×10^{20} μ/year for an acceptance of 0.074 eVs and 1.5 π cm rad.

	0.0185 eVs 1.5 π cm rad	0.074 eVs 1.5 π cm rad
rotation	4.6×10^{19}	1.3×10^{20}
44 MHz	4.4×10^{19}	9.1×10^{19}
88 MHz	4.0×10^{19}	8.8×10^{19}
176 MHz	3.8×10^{19}	5.9×10^{19}

Table 6: Muons per year within recirculator acceptance at different stages of the front-end.

7 Conclusions and Future Work

It has been shown that an optimized muon front-end without cooling can provide roughly one order of magnitude less muons than the CERN reference scenario with cooling.
The numbers given in Section 6 represent the present status of this work. Further work will include different modeling of the solenoid fields as well as optimized transverse matching.
Furthermore, future simulations should be run at higher statistics, since the numbers quoted in Tab. 6 have been extrapolated from small numbers of muons found at the end of the channel and are hence subject to fluctuations.

8 Acknowledgements

I would like to thank G. Franchetti, E. Keil, A. Lombardi and S. Russenschuck for helpful discussions.

References

[1] A. Lombardi, *A 40-80 MHz System for Phase Rotation and Cooling*, CERN Neutrino Factory Note 34 (2000).
[2] K. Hanke, *Muon Capture and Acceleration without Phase Rotation and Cooling*, CERN Neutrino Factory Note 39, (2000).
[3] Simulation Code *PATH*, CERN version.
[4] E. Keil, private communication.
[5] E. Keil, *Muon Recirculating Linear Accelerator Design*, transparencies shown in the NFWG meeting of April 19, 2000, p. 9.
http://nfwg.home.cern.ch/nfwg/nufactwg/23/min19apr00.htm
[6] E. Keil, *A 50 GeV Muon Storage Ring Design*, CERN SL-2000-013 (AP) and CERN Neutrino Factory Note 26, p.15, (2000).
[7] N. Vassilopoulos, private communication.
[8] S. Russenschuck, private communication.
[9] G. Franchetti, private communication.